Coherent angular motion in the establishment of multicellular architecture of glandular tissues

Kandice Tanner[1], Hidetoshi Mori, Rana Mroue, Alexandre Bruni-Cardoso, and Mina J. Bissell[1]

Life Sciences Division, Lawrence Berkeley National Laboratory, Berkeley, CA 94720

Contributed by Mina J. Bissell, November 30, 2011 (sent for review November 9, 2011)

Glandular tissues form ducts (tubes) and acini (spheres) in multicellular organisms. This process is best demonstrated in the organization of the ductal tree of the mammary gland and in 3D models of morphogenesis in culture. Here, we asked a fundamental question: How do single adult epithelial cells generate polarized acini when placed in a surrogate basement membrane 3D gel? Using human breast epithelial cells from either reduction mammoplasty or nonmalignant breast cell lines, we observed a unique cellular movement where single cells undergo multiple rotations and then maintain it cohesively as they divide to assemble into acini. This coherent angular motion (CAMo) was observed in both primary cells and breast cell lines. If CAMo was disrupted, the final geometry was not a sphere. The malignant counterparts of the human breast cell lines in 3D were randomly motile, did not display CAMo, and did not form spheres. Upon "phenotypic reversion" of malignant cells, both CAMo and spherical architecture were restored. We show that cell-cell adhesion and tissue polarity are essential for the formation of acini and link the functional relevance of CAMo to the establishment of spherical architecture rather than to multicellular aggregation or growth. We propose that CAMo is an integral step in the formation of the tissue architecture and that its disruption is involved in malignant transformation.

actin dynamics | cancer | cell migration | multicellular assembly | cellular rotation

Epithelial organs form elaborate architectures consisting of ducts and acini in kidney, lung, salivary- and mammary- glands in vertebrates and invertebrates alike (1, 2). In tissues, loss of polarity markers is one of the earliest changes detected during malignant transformation (3, 4). The terminal unit of the arboreal tree, the acinus, was robustly recapitulated in 3D cultures of the mammary epithelial in laminin-rich gels (lrECM), where cells divide and organize into growth-arrested polarized spheres with basolateral and apical membrane domains surrounding a central lumen (5, 6). These models have shown the differential response of preinvasive and malignant epithelial cells to lrECM, where cells no longer form acini but aggregate into nonpolarized geometries similar to neoplastic lesions and tumors in vivo (6–11). To understand how tissue polarity and architecture are lost during transformation, one needs to first understand how the normal cells are able to form acini. However, the processes by which a single epithelial cell is able to recapitulate polarized structures that resemble structural units of function in 3D gels and in vivo are not known. We hypothesized that adult cells undergo a specific morphogenetic program to form and maintain quiescent acini, and that this program is corrupted in malignant transformation.

Using real-time imaging and lrECM gels, we uncovered a unique cellular movement where single breast epithelial cells completed multiple rotations that were maintained as they divided to assemble into acini. This movement is reminiscent of cellular behavior governing organ formation in early developmental stages of *Xenopus* and Helisoma embryos (12, 13), described more than two decades ago. That this embryonic process could be maintained in adult human cells in 3D gels is both surprising and exciting, and may provide a possible explanation for how the adult mammary gland after each pregnancy and involution can reorganize the epithelial tree (14).

On the other hand, malignant cells were randomly motile in lrECM gels on their way to form disorganized structures. Upon "phenotypic reversion" (11), however, they reentered the morphogenetic program to regain basally polarized structures. This switch suggested that there is a differential activation of motility signaling programs when malignant cells are phenotypically "normalized."

In this article, we functionally link the coherent angular motion (CAMo) to the establishment of multicellular polarized spheres. We describe the relationship between tissue polarity, cell-cell adhesion, and cell movement, and determine the role of actomyosin structures and myosin light-chain–regulated forces on the establishment of the acinar structures. We also show the disintegration of these pathways in the malignant behavior of breast cancer cells, thus reinforcing the notion that coherent cellular movement within an ECM cocoon guides formation of structural units of tissues important for quiescence and homeostasis.

Results

To address the question of how single mammary cells can reestablish polarized acini in 3D lrECM, we used human mammary epithelial cells (HMECs) from both reduction mammoplasties and nonmalignant breast cell lines (S1-HMT3522 and MCF10A), as previously described (6, 7, 15). Single HMECs were imaged with confocal fluorescence microscopy continuously for 4 d; they underwent multiple rotations (~0.5–1 revolution per hour), and then continued to rotate cohesively as they and their progenies divided (Fig. 1*A* and Movies S1, S2, and S3). The observed chirality was random, suggesting that there were no directional preference for spherical formation under culture conditions used here. Individual nuclei (Fig. 1*B*), as well as the entire cluster, rotated with the angular velocity increasing as a function of cell size up to the four-cell stage (Fig. 1*C*). We named this global movement where cells coupled with the nearest neighbors rotated as a cohesive unit CAMo.

To determine whether CAMo was a driver of acinar morphogenesis or was simply a consequence of 3D multicellular aggregation, we compared the cellular movements of acini vs. aggregates. Acini grown from freshly excised single primary HMEC cells coherently rotated (Fig. 1*E*, *Left*, Fig. S1, and Movie S4), whereas cells preaggregated into clusters of ~20 cells before culturing in 3D were randomly motile (Fig. 1*E*, *Right*, and Movie S5) (16). Our finding that CAMo was observed only when acini evolved from a single cell suggests that self-generated centripetal forces are integral to the establishment of spherical geometry in lrECM gels.

Author contributions: K.T. and M.J.B. designed research; K.T., H.M., R.M., and A.B.-C. performed research; K.T. analyzed data; and K.T. and M.J.B. wrote the paper.

The authors declare no conflict of interest.

Freely available online through the PNAS open access option.

[1]To whom correspondence may be addressed. E-mail: ktanner@lbl.gov or mjbissell@lbl.gov.

This article contains supporting information online at www.pnas.org/lookup/suppl/doi:10.1073/pnas.1119578109/-/DCSupplemental.

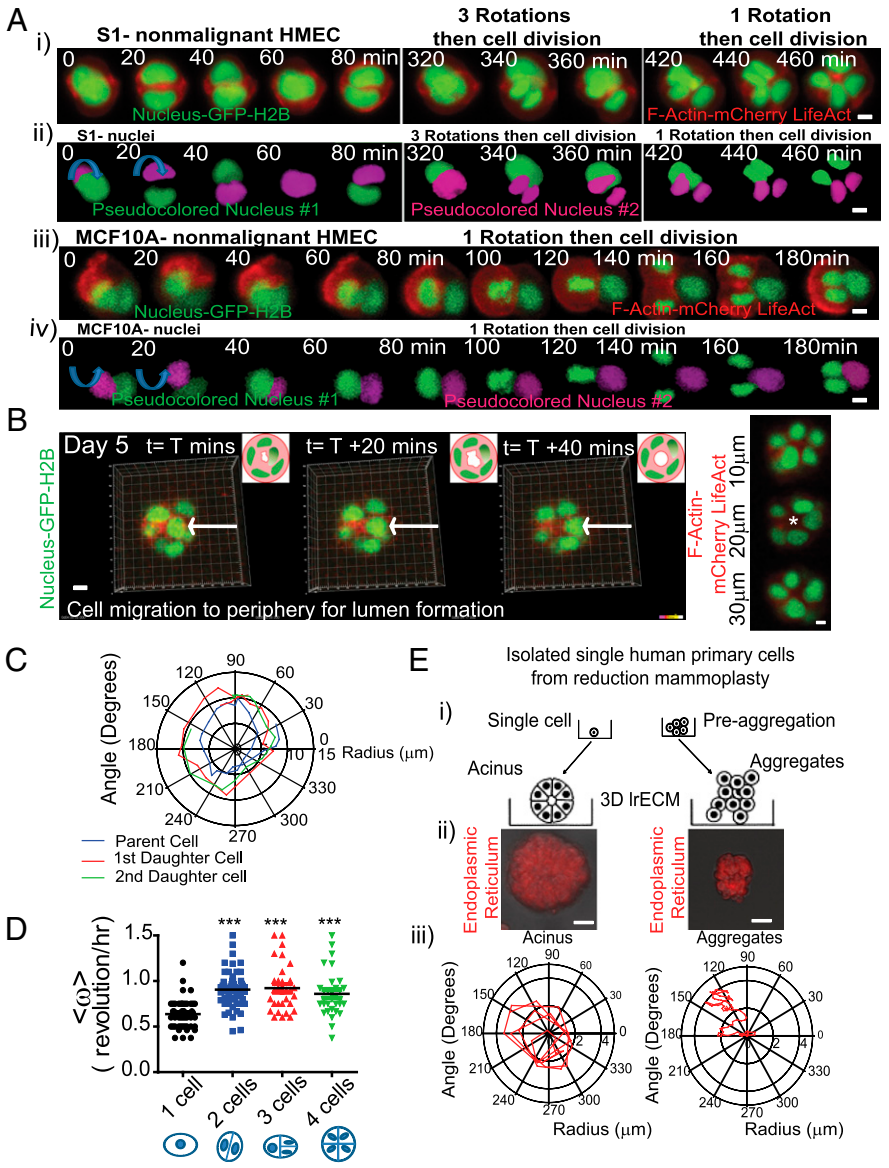

Fig. 1. (*A*) Nonmalignant cell lines undergo multiple rotations during mammary acinar morphogenesis. (*i*) Timed micrographs of S1 cells show the ordered development of multicellular aggregates as revealed by nuclear position and F-actin. Cells undergo multiple rotations before mitosis. (*ii*) Same micrographs as in *i* but showing only nuclei where one is false-colored purple. Blue arrows indicate the direction of rotation. (*iii*) Timed micrographs of MCF10A cells show comparable evolution of the structure. (*iv*) Same micrographs as in *iii*, but showing only nuclei, as described for *ii*. (Scale bars, 10 µm.) (*B*) Timed micrographs from conclusion of acinar morphogenesis (day 5) of S1 cells where the final structure (10 cells) form a lumen. Color coded for time: blue (0 h) to red (40 min). (*Inset*) Schematic. (*Right*) Cross section at different planes. (Scale bar, 30 µm.) * indicates lumen. (*C*) Angular rotation of the parent cell and its progeny by tracking the individual nuclei during acinar morphogenesis. (*D*) Average angular velocity as a function of increasing number of cells comprising multicellular structure. Using Mann–Whitney *U* test where $P < 0.0001$. (*E, i*) Schematic of experimental design. (*ii*) Micrographs showing acinus (8 d) (*Left*). (*Right*) The aggregates (6 h). Red represents the endoplasmic reticulum. (Scale bars, 50 µm.) (*iii*) Graphs comparing acinus vs. aggregates for a period of 24 h.

If indeed CAMo were central to formation of acini, it would follow that this morphogenetic program would be compromised in malignant cells because these cells do not form polarized acini (6, 11). Following the logic through, when malignant cells are phenotypically reverted to form acini-like structures (11; reviewed in 17), CAMo would have to be restored to allow formation of acini. To test the above hypothesis, we used an isogenic model of breast cancer progression, the HMT3522 series, where cells from reduction mammoplasty, were grown in defined medium and were spontaneously immortalized but remained nonmalignant (S1); upon removal of the sole growth factor, EGF, a malignant population (T4-2) emerged after injection into mice without addition of exogenous oncogenes (9, 18). We showed previously that these cells can be phenotypically reverted in 3D lrECM, where spherical structure is regained, even though these cells are "genotypically malignant" (9, 11). When seeded in lrECM, both single nonmalignant and malignant cells rotated, but malignant cells displayed higher centripetal velocities (Fig. 2*Ai*). The differential motility we observed between nonmalignant and malignant cells suggests that individual cell dynamics could be predictive of neoplastic transformation, even when cells are removed from the tissue.

The temporal window wherein phenotypic reversion of the malignant cells is obtained is restricted to the first 36–48 h in 3D cultures independently of the pharmacological agents used for reversion. This motivated the present studies whereby the

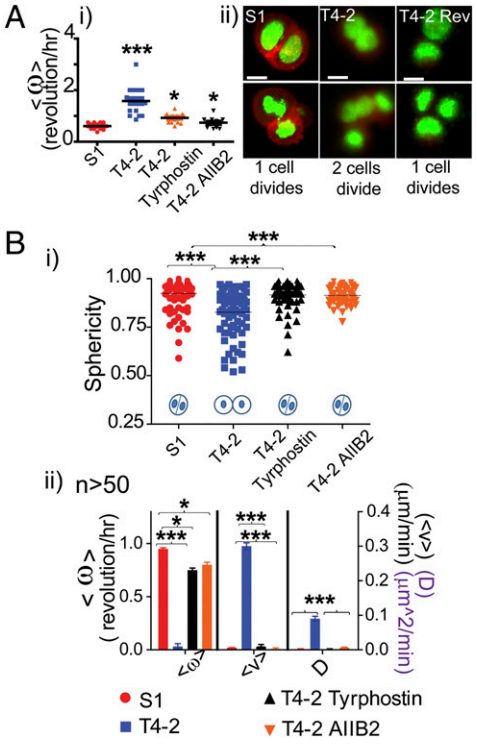

Fig. 2. Early acinar morphogenesis: motility, actin dynamics, and mitosis for single cells, and the first division for HMT3522 series. (*A*, *i*) Graph quantifying the average angular motion for single cells. ***$P < 0.0001$ and *$P < 0.01$. (*ii*) Micrographs showing cell division for S1, T4-2, and T4-2 rev. (Scale bars 10 μm.) (*B*, *i*) Comparison of cell adhesion measured by sphericity of the cell aggregates, ***$P < 0.0001$. (*ii*) Graph depicting different types of motility for HMT3222 series using Student *t* test, *$P < 0.01$ and ***$P < 0.0001$.

cellular reprogramming commitment required for reversion to acini-like structures has to be activated within this window. S1 and reverted-T4-2 (T4-2 Rev) cells exhibited staggered divisions with a delay between the second and third mitoses (Fig. 2*Aii*, *Left* and *Right*, and Table S1).On the other hand, T4-2 cells displayed no such delay (Fig. 2*Aii*, *Center*, Table S1, and Movie S6). This temporal difference suggested that the nonmalignant cells might use this delay to assemble adhesions required for the scaffold that allows them to form polarized acini.

We observed a shift in cell adhesion as measured by both sphericity and cellular movements after the first cell division during this "reversion window" (Fig. 2*B*). The S1 cells continued to exhibit CAMo as they formed spheres (Movie S7), whereas the T4-2 cells were loosely tethered, lacked CAMo, and became randomly motile (Fig. 2*B* and Movie S8), supporting the notion that the observed delays in timing of division may be important in establishment of functional cell-cell adhesions in S1 and T4-2 Rev cells (Movie S9). Both S1 and T4-2 Rev cells continued CAMo past this critical window, and T4-2 cells continued to be randomly motile (Fig. S2, and Movies S10, S11, S12, and S13). Thus, the type of cellular motion that cells undergo during early morphogenesis drives the final structure of the tissue. Using the MCF10a series, we confirmed that both cell adhesion and CAMo were maintained also for the nonmalignant MCF10a after the first cell division, but that these features were lost as a function of progression to malignancy (Fig. S3, Table S2, and Movies S14 and S15). Thus, the correlation between CAMo and normal morphogenesis and its loss as cells become malignant are conserved from primary normal cells to HMT3522 and MCF10a breast cancer series.

Tissue polarity is established via a temporally modulated multistage process regulated by the mammary microenvironment (17). There is evidence to indicate that growth and tissue polarity are separable in formation of polarized acini in 3D (19–21). Specifically, we showed that Akt and Rac1 act as downstream effectors of PI3K and function as separate pathways for cellular proliferation and tissue polarity, respectively (20). Partitioning deficient 3 homolog (PAR3), a key component of tight junctions (22, 23), is expressed differentially at both gene (*PARD3*) and protein (PAR3) levels in S1 and T4-2 cells (Fig. 3*A* and Fig. S4). To determine the relationship between loss of CAMo and disruption of acinar polarity, we silenced PARD3 using shRNA in nonmalignant cells. Both CAMo and acinar structures were compromised where cells formed nonpolarized, grape-like structures, supporting the notion that angular motility and tissue polarity are reciprocally connected (Fig. 3 *B* and *C*, and Movie S16). Similarly, interrogation of the role of E-Cadherin via a function-blocking antibody (24) compromised CAMo and, hence, acinar structure, emphasizing again the importance of cell-cell adhesion for maintenance of CAMo (Fig. 3 *A iv* and *v*, *B*, and *C*).

The dynamic properties of actomyosin networks and microtubules have been shown to regulate cell motility and balance cellular forces (25). Pharmacological destabilization of microtubules did not inhibit single-cell centripetal motion (Fig. S5); thus, the switch from CAMo to random motility would predict differential spatiotemporal regulation of actomyosin. We first visualized actin dynamics using HMT3522 series transduced with mCherry LifeAct lentivirus (26). As early as 4 h postseeding in lrECM, a crescent-shaped cortical actin was established as if directing the angular motion (Fig. 4*A* and Movie S17). After the first cell division, the polarized cortical actin was retained in the S1 and T4-2 Rev cells (Fig. 4*B*, *i* and *iii*), but became randomly distributed around the membranes in T4-2 cells (Fig. 4*Bii*), supporting a predictable connection between actin and CAMo.

To further identify the molecular components of the actomyosin network that contribute to CAMo, we targeted the networks' effectors, Myosin II, myosin light-chain kinase (MLCK), and Rho-associated kinase (ROCK) using pharmacological inhibitors (27–30). Because Rho-regulated contractile forces influence cell proliferation (31), we determined the appropriate titer of the inhibitor where cell proliferation was not—or minimally—affected. This determination allowed us to modulate the activity of myosin light chain without affecting growth. It is known that phosphorylation of myosin light chain-2 (MLC2) at threonine 18 and serine 19 (16) is involved in the motility of several cancer cell lines (32). We reasoned that by modulating MLC2 in nonmalignant S1 cells, we might be able to mimic motility of malignant T4-2 cells. Treatment with vehicle control confirmed that CAMo was unaffected (Fig. 4*C Top*, and Movie S18), whereas all three inhibitors disrupted CAMo. Addition of Blebbistatin, an inhibitor of Myosin II (33), led to random motility and resulted in formation of stellate structures (Fig. 4*C*, *2nd Panel*, and Movies S19 and S20). The MLCK inhibitor, ML-7, also caused random motility, but cells formed aggregates rather than stellates (Fig. 4*C*, *3rd Panel*, and Movies S21 and S22). ROCK inhibition, using Y-27632 (34), strongly reduced motility leading to formation of flattened discs (Fig. 4*C*, *Bottom*, and Movies S23 and S24). These data suggested that all three pathways are involved in regulation of CAMo. However, inhibition of each component led to formation of different structures and activity levels of MLC2 (Fig. 4*D*, *ii* and *iii*), further linking final structure to the type of motility determined by which components of the actomyosin program are active in cells forming the organs.

Discussion

Using 4D live imaging, we report a unique cellular movement, CAMo, by which acinar morphogenesis is made possible in 3D lrECM. Single adult human breast epithelial cells undergo multiple rotations, and then continue to divide cohesively to achieve

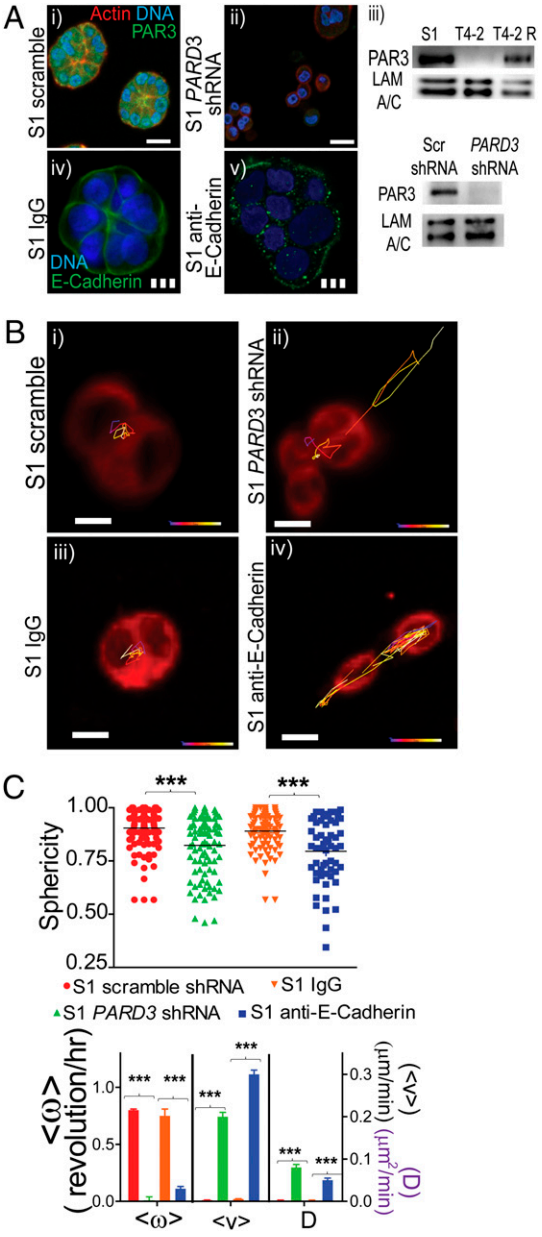

Fig. 3. The role of cell-cell adhesion and polarity proteins in CAMo. (*A*, *i* and *ii*) Immunofluorescence of actin, Par3, and DNA for S1 scramble and S1PAR3 shRNA. (Solid scale bar, 10 μm.) (*iii*) Immunoblots comparing protein levels. (*iv* and *v*) E-Cadherin immunofluorescence for S1 IgG and S1s cells anti–E-Cadherin. (Dashed scale bar, 20 μm.) (*B*) Micrographs show S1 Scramble (*i*), S1 PARD3 (*ii*), S1 IgG (*iii*), and S1 anti-E-Cadherin (*iv*), color coded for time: blue (0 h) to red (12 h); at the two-cell level, red is the endoplasmic reticulum. (*C*, *Upper*) Graph shows comparison of sphericity of the cell aggregates. ***$P < 0.0001$. (*Lower*) Graph depicting different types of motility for S1 scramble and S1IgG, which still rotate although S1 PAR3 shRNA and S1 anti–E-Cadherin undergo a combination of linear velocity as well as random motion. Student *t* test, where ***$P < 0.0001$.

assembly into acini. Malignant cells do not exhibit CAMo and form disorganized structures in 3D. A unique and possibly related morphogenetic movement and program recently described by Haigo and Bilder (35) was shown to facilitate the transition of the geometry of the *Drosophila* follicle from that of a sphere to an ellipse. The description of the embryonic movement reinforces the notion that under appropriate contexts, adult cells may engage the embryonic morphogenetic programs to reestablish their tissue structure with the mammary gland as a prime example.

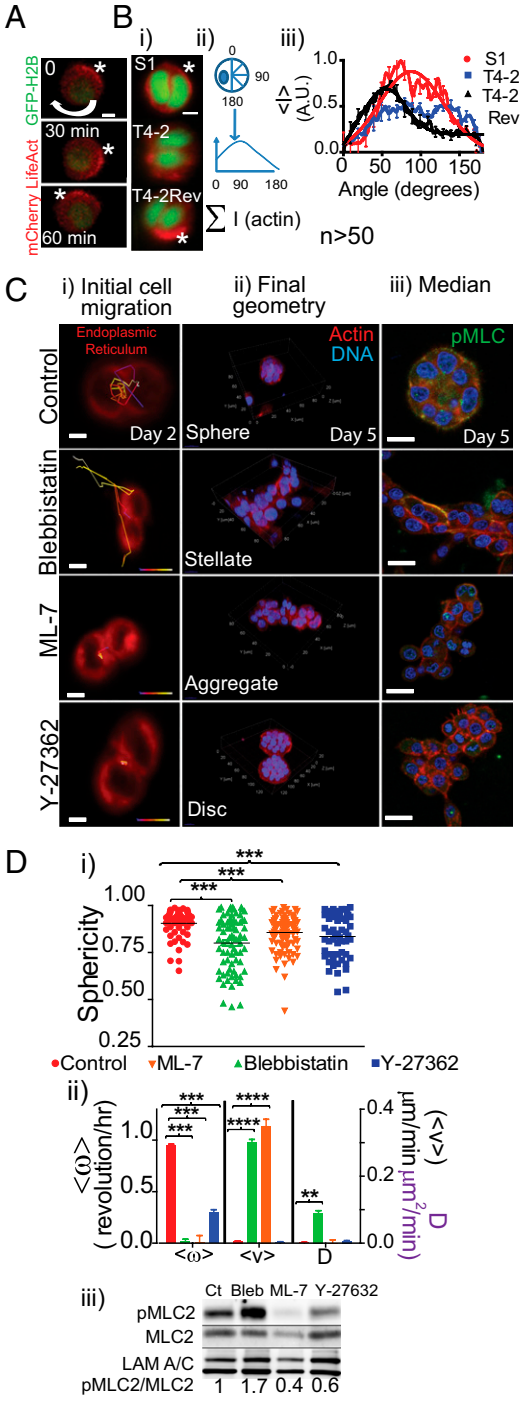

Fig. 4. Initial cellular motion dictates final structure where only cells that undergo and maintain CAMo eventually form an acinus. (*A*) Micrographs of peripheral actin front, denoted by the white asterisk. (Scale bars, 10 μm.) (*B*, *i*) Micrographs show peripheral actin at the two-cell stage. (Scale bars, 20 μm.) (*ii*) Schematic of the method of quantification of the spatial distribution of actin. (*iii*) Average spatial actin distribution at the two-cell stage. Solid line, Gaussian approximation. (*C*) Pharmacological treatment of S1 shown with time stamped micrographs. (*i*) Cell tracking, color-coded (blue to red denotes increasing time). Red, endoplasmic reticulum. (Scale bars, 10 μm.) Trajectories in *i* show final architecture in *ii*. (*iii*) Median cross-section for actin (red), pMLC (green), and DAPI (blue). (*D*, *i*) Graph comparing sphericity, ***$P < 0.0001$. (*ii*) Comparison of motilities: ****$P < 0.00001$, ***$P < 0.0001$, and **$P < 0.001$. (*iii*) Immunoblots of pMLC, MLC, and Lamin A/C (internal control).

In our assay, nonmalignant and reverted malignant cells divided with a significant delay between the second and third mitoses, whereas loosely tethered malignant cells showed no such delay, suggesting that the timing delay may be needed to facilitate formation of cell-cell adhesions and the scaffold on which the tissue structure would be built. That "timing" has important functional consequences was described by Wong et al., who showed that if the duration of mitosis during human blastocyst formation was altered in any direction, the resultant embryo would be abnormal (36).

Not surprisingly, blocking E-Cadherin function disrupted cell-cell and to a lesser extent, cell-ECM adhesion, in turn impairing CAMo (Fig. 3). E-Cadherin plays a role in establishing and maintaining epithelia during development, from early embryogenesis through the later stages of organogenesis, as shown in *Drosophila* and E-Cadherin knockout mouse models (37–39). CAMo was also blocked by down-regulating PAR3, required in establishing polarity of epithelial tissues (22, 23). These data, coupled with the observation that malignant cells are randomly motile during formation of disorganized structures but perform CAMo upon phenotypic reversion, suggest that CAMo drives, or at least contributes, to tissue polarity.

Real-time visualization of actin dynamics revealed that crescent-shaped cortical actin may direct centripetal motion. Such localization differs from anterior-posterior asymmetry of actin polarization studied on other surfaces (40). However, all underlie the importance of the actomyosin structures in generating motion. We observed here that single epithelial cells are able to rotate with little translocation in lrECM, thus extending the known repertoire of cell motilities. Tumor cells can switch between mesenchymal (16, 41) and amoeboid (16, 42) movements, regulated by ROCK and Rac, respectively, and proteolytic activity for single-cell invasion in collagen gels (42). In our system, additional experiments are required to determine if there is localized ECM degradation or rapid turnover of cell-ECM adhesions to facilitate rotation within lrECM.

Cells can modulate their force generation as a response to local extracellular stiffness, where the malignant transformation is regulated in vitro and in vivo by stiffening the ECM (43, 44). Using sustained pharmacological inhibition of Myosin II, ROCK, and MLCK, we modulated activity of MLC2 in nonmalignant cells. This process disrupted the generation of centripetal forces, resulting in establishment of nonpolar structures, reinforcing the bidirectional relationship between physical and biochemical control of malignancy. Thus, myosin-regulated centripetal force can be added to the repertoire of known mechanisms by which cells can navigate their 3D microenvironment.

Previous studies in adult cell lines have shown rotating nuclei within static cells in 2D (45–47). A mathematical method was used to distinguish between random and centripetal motility during real-time visualization of lumen initiation in Madin-Darby canine kidney cell aggregates on the order of minutes (48), and inducible activation of ERK1/2 of nonmalignant epithelial cells within mature acini was shown to promote cell motility for several hours, disrupting epithelial architecture (49). These exciting findings reveal the potency of direct visualization to unravel and decipher novel cellular dynamics. Moreover, our visualization of the full acinar morphogenesis revealed the functional link between type of motility and realized structure. Continued visualization of the evolution of other tissues and forms may reveal an evolutionarily conserved mechanism by which cellular architecture is established and governed.

Materials and Methods

HMT3522 and MCF10A series (6–8), primary HMEC, kindly provided by William Curt Hines (Lawrence Berkeley National Laboratory, Berkeley, CA) and obtained from the University of California at San Francisco Cancer Center and the Cooperative Human Tissue Network, were cultured as previously described, and 3D samples gelled on glass chambers (Nalge Nunc) (7, 8, 15). Stable cell lines expressing mCherry LifeAct and H2B-GFP, and PAR3 KD cells were created (*SI Materials and Methods*). ER-tracker-mCherry (Invitrogen) was added to the medium (1:1,000) for 30 min and replaced before imaging.

Before imaging, 5 μM Y-27632 (Calbiochem), 25 μM Blebbistatin, 0.5 μM ML-7 (Sigma), 200 μg/mL mouse anti–E-Cadherin, or anti-IgG Human (Invitrogen), respectively, were supplemented 5% lrECM/media (vol/vol) for 2 h. Media mixture was refreshed at day 3. At day 5, samples were fixed and stained as previously described (8) (*SI Materials and Methods*).

Images were acquired at one frame per second with an upright Zeiss LSM 710. Images were of 134.9 × 134.9 μm^2 lateral dimensions, axial displacement of 75 μm (step size 0.5 μm) imaged with a 1.4 NA 63× oil-immersion objective, sequentially using 405 nm and 488 nm (respectively) lines from an argon ion laser and 546 nm from a solid-state laser. Emission BP filters were set for 450–465 nm, 505–525 nm, and 560–575 nm at a gain of 400. Four-dimensional images of dimensions 701 × 701 μm^2 lateral dimensions, axial displacement of 150 μm (axial step size, 2 μm), were imaged with a 0.8 NA 20× air objective at ∼one frame per second. A time interval of 20 min was programmed after one *z* stack for 4 d. Samples were maintained at 37 °C and 5% CO_2.

Image Processing. Images were exported using Zen 2009 software and ImageJ for display. Three-dimensional volume rendering and cell tracking were performed using object tracking and surface rendering algorithms in Bitplane Imaris software. For multicellular structures, individual cell traces excluding mitosis were used to calculate the angular velocity and mean square displacement (MSD). The sphericity, Ψ (50),

$$\Psi = \frac{\pi^{\frac{1}{3}}(6V_p)^{\frac{2}{3}}}{A_p} \quad [1]$$

where V_p is volume of the particle and A_p is the surface area of the particle. Single cell/centroid trajectories were analyzed as previously described (51). MSD (τ) was calculated for (τ) of one-quarter of total data points:

$$\mathrm{MSD}(\tau) = \langle (x(t) - x(t+\tau))^2 + (y(t) - y(t+\tau))^2 + (z(t) - z(t+\tau))^2 \rangle. \quad [2]$$

following fitting parameters to the trajectories (51).

$$\mathrm{MSD}(\tau) = 6D\tau \quad [3]$$

$$\mathrm{MSD}(\tau) = 6D\tau + (v\tau)^2, \quad [4]$$

D is the diffusion coefficient and *v* is velocity.

Statistical Analysis. Bar graphs are shown as mean with SEs for trajectory analysis and a Student *t* test (unpaired, two-tailed, 95% confidence interval) was used to determine statistical significance. For sphericity analysis, distributions were not Gaussian (as confirmed by the Bartlett's test); using nonparametric methods, we employed a two-sided Mann–Whitney test.

ACKNOWLEDGMENTS. We thank Daniel Fletcher, Ramray Bhat, Alexander Borowsky, Jamie Bascom, Irene Kuhn, Joni Mott, and Mandana Vesieh for critical reading of the manuscript; Jamie Inman, Aaron Boudreau, Eva H. Lee, and Myan Do for initial assistance; William Curt Hines for kindly providing human tissue; and Douglas Brownfield, Ana Coreia, Cyrus Ghajar, Eileen Koh, Alvin T. Lo, Michelle Scott, and Damir Sudar for their helpful comments. This work was supported in part by postdoctoral Fellowship W81XWH-09-1-0666 (to K.T.) and predoctoral Fellowship W81XWH-08-1-0481 (to R.M.) from the US Department of Defense Breast Cancer Research Program. The work from M.J.B.'s laboratory is supported by grants from the US Department of Energy, Office of Biological and Environmental Research, a Distinguished Fellow Award, and Low Dose Radiation Program Contract DE-AC02-05CH1123; National Cancer Institute Awards R37CA064786, U54CA126552, U54CA112970, U01CA143233, and NCI U54CA143836 (Bay Area Physical Sciences–Oncology Center, University of California, Berkeley, CA); and the US Department of Defense (W81XWH0810736).

1. Chuong C-M (1998) *Molecular Basis of Epithelial Appendage Morphogenesis. Molecular Biology IntelligenceUunit* (R.G. Landes, Austin, TX).

2. Lu P, Werb Z (2008) Patterning mechanisms of branched organs. *Science* 322: 1506–1509.

3. Namba R, et al. (2004) Molecular characterization of the transition to malignancy in a genetically engineered mouse-based model of ductal carcinoma in situ. *Mol Cancer Res* 2:453–463.
4. Bloom HJ, Richardson WW (1957) Histological grading and prognosis in breast cancer; A study of 1409 cases of which 359 have been followed for 15 years. *Br J Cancer* 11: 359–377.
5. Barcellos-Hoff MH, Aggeler J, Ram TG, Bissell MJ (1989) Functional differentiation and alveolar morphogenesis of primary mammary cultures on reconstituted basement membrane. *Development* 105:223–235.
6. Petersen OW, Rønnov-Jessen L, Howlett AR, Bissell MJ (1992) Interaction with basement membrane serves to rapidly distinguish growth and differentiation pattern of normal and malignant human breast epithelial cells. *Proc Natl Acad Sci USA* 89: 9064–9068.
7. Debnath J, Muthuswamy SK, Brugge JS (2003) Morphogenesis and oncogenesis of MCF-10A mammary epithelial acini grown in three-dimensional basement membrane cultures. *Methods* 30:256–268.
8. Lee GY, Kenny PA, Lee EH, Bissell MJ (2007) Three-dimensional culture models of normal and malignant breast epithelial cells. *Nat Methods* 4:359–365.
9. Rizki A, et al. (2008) A human breast cell model of preinvasive to invasive transition. *Cancer Res* 68:1378–1387.
10. Kenny PA, et al. (2007) The morphologies of breast cancer cell lines in three-dimensional assays correlate with their profiles of gene expression. *Mol Oncy* 1(1): 84–96.
11. Weaver VM, et al. (1997) Reversion of the malignant phenotype of human breast cells in three-dimensional culture and in vivo by integrin blocking antibodies. *J Cell Biol* 137:231–245.
12. Gerhart J, et al. (1989) Cortical rotation of the *Xenopus* egg: Consequences for the anteroposterior pattern of embryonic dorsal development. *Development* 107(Suppl): 37–51.
13. Diefenbach TJ, Koehncke NK, Goldberg JI (1991) Characterization and development of rotational behavior in Helisoma embryos: Role of endogenous serotonin. *J Neurobiol* 22:922–934.
14. Medina D (1996) The mammary gland: A unique organ for the study of development and tumorigenesis. *J Mammary Gland Biol Neoplasia* 1:5–19.
15. Stampfer M, Hallowes RC, Hackett AJ (1980) Growth of normal human mammary cells in culture. *In Vitro* 16:415–425.
16. Friedl P, Wolf K (2003) Tumour-cell invasion and migration: Diversity and escape mechanisms. *Nat Rev Cancer* 3:362–374.
17. Bissell MJ, Kenny PA, Radisky DC (2005) Microenvironmental regulators of tissue structure and function also regulate tumor induction and progression: The role of extracellular matrix and its degrading enzymes. *Cold Spring Harb Symp Quant Biol* 70: 343–356.
18. Briand P, Petersen OW, Van Deurs B (1987) A new diploid nontumorigenic human breast epithelial cell line isolated and propagated in chemically defined medium. *In Vitro Cell Dev Biol* 23:181–188.
19. Aranda V, et al. (2006) Par6-aPKC uncouples ErbB2 induced disruption of polarized epithelial organization from proliferation control. *Nat Cell Biol* 8:1235–1245.
20. Liu H, Radisky DC, Wang F, Bissell MJ (2004) Polarity and proliferation are controlled by distinct signaling pathways downstream of PI3-kinase in breast epithelial tumor cells. *J Cell Biol* 164:603–612.
21. Beliveau A, et al. (2010) Raf-induced MMP9 disrupts tissue architecture of human breast cells in three-dimensional culture and is necessary for tumor growth in vivo. *Genes Dev* 24:2800–2811.
22. Etienne-Manneville S, Hall A (2003) Cell polarity: Par6, aPKC and cytoskeletal crosstalk. *Curr Opin Cell Biol* 15:67–72.
23. Martín-Belmonte F, et al. (2008) Cell-polarity dynamics controls the mechanism of lumen formation in epithelial morphogenesis. *Curr Biol* 18:507–513.
24. Ribeiro AS, et al. (2010) Extracellular cleavage and shedding of P-cadherin: A mechanism underlying the invasive behaviour of breast cancer cells. *Oncogene* 29:392–402.
25. Ingber DE (2003) Tensegrity I. Cell structure and hierarchical systems biology. *J Cell Sci* 116:1157–1173.
26. Tanner K, Boudreau A, Bissell MJ, Kumar S (2010) Dissecting regional variations in stress fiber mechanics in living cells with laser nanosurgery. *Biophys J* 99:2775–2783.
27. Allen WE, Jones GE, Pollard JW, Ridley AJ (1997) Rho, Rac and Cdc42 regulate actin organization and cell adhesion in macrophages. *J Cell Sci* 110:707–720.
28. Ridley AJ, Hall A (1994) Signal transduction pathways regulating Rho-mediated stress fibre formation: Requirement for a tyrosine kinase. *EMBO J* 13:2600–2610.
29. Amano M, et al. (1997) Formation of actin stress fibers and focal adhesions enhanced by Rho-kinase. *Science* 275:1308–1311.
30. Geiger B, Bershadsky A, Pankov R, Yamada KM (2001) Transmembrane crosstalk between the extracellular matrix—Cytoskeleton. *Nat Rev Mol Cell Biol* 2:793–805.
31. Provenzano PP, Keely PJ (2011) Mechanical signaling through the cytoskeleton regulates cell proliferation by coordinated focal adhesion and Rho GTPase signaling. *J Cell Sci* 124:1195–1205.
32. Sahai E, Marshall CJ (2003) Differing modes of tumour cell invasion have distinct requirements for Rho/ROCK signalling and extracellular proteolysis. *Nat Cell Biol* 5: 711–719.
33. Kovács M, Tóth J, Hetényi C, Málnási-Csizmadia A, Sellers JR (2004) Mechanism of blebbistatin inhibition of myosin II. *J Biol Chem* 279:35557–35563.
34. Ishizaki T, et al. (2000) Pharmacological properties of Y-27632, a specific inhibitor of rho-associated kinases. *Mol Pharmacol* 57:976–983.
35. Haigo SL, Bilder D (2011) Global tissue revolutions in a morphogenetic movement controlling elongation. *Science* 331:1071–1074.
36. Wong CC, et al. (2010) Non-invasive imaging of human embryos before embryonic genome activation predicts development to the blastocyst stage. *Nat Biotechnol* 28: 1115–1121.
37. Larue L, et al. (1994) E-cadherin null mutant embryos fail to form a trophectoderm epithelium. *Proc Natl Acad Sci USA* 91:8263–8267.
38. Tepass U, et al. (1996) shotgun encodes *Drosophila* E-cadherin and is preferentially required during cell rearrangement in the neurectoderm and other morphogenetically active epithelia. *Genes Dev* 10:672–685.
39. Tunggal JA, et al. (2005) E-cadherin is essential for in vivo epidermal barrier function by regulating tight junctions. *EMBO J* 24:1146–1156.
40. Lauffenburger DA, Horwitz AF (1996) Cell migration: A physically integrated molecular process. *Cell* 84:359–369.
41. Doyle AD, Wang FW, Matsumoto K, Yamada KM (2009) One-dimensional topography underlies three-dimensional fibrillar cell migration. *J Cell Biol* 184:481–490.
42. Sanz-Moreno V, et al. (2008) Rac activation and inactivation control plasticity of tumor cell movement. *Cell* 135:510–523.
43. Paszek MJ, et al. (2005) Tensional homeostasis and the malignant phenotype. *Cancer Cell* 8:241–254.
44. Levental KR, et al. (2009) Matrix crosslinking forces tumor progression by enhancing integrin signaling. *Cell* 139:891–906.
45. Englander LL, Rubin LL (1987) Acetylcholine receptor clustering and nuclear movement in muscle fibers in culture. *J Cell Biol* 104:87–95.
46. Pomerat CM (1953) Rotating nuclei in tissue cultures of adult human nasal mucosa. *Exp Cell Res* 5:191–196.
47. Ji JY, et al. (2007) Cell nuclei spin in the absence of lamin b1. *J Biol Chem* 282: 20015–20026.
48. Marmaras A, et al. (2010) A mathematical method for the 3D analysis of rotating deformable systems applied on lumen-forming MDCK cell aggregates. *Cytoskeleton (Hoboken)* 67:224–240.
49. Pearson GW, Hunter T (2007) Real-time imaging reveals that noninvasive mammary epithelial acini can contain motile cells. *J Cell Biol* 179:1555–1567.
50. Wadell H (1935) Volume, shape, and roundness of quartz particles. *J Geol* 43:250–280.
51. Saxton MJ, Jacobson K (1997) Single-particle tracking: Applications to membrane dynamics. *Annu Rev Biophys Biomol Struct* 26:373–399.